International Journal of Robotics and Control Systems
Vol. 5, No. 2, 2025, pp. 1102-1119
ISSN 2775-2658
http://pubs2.ascee.org/index.php/ijrcs

A Morphological Context Blocks Hybrid CNN for Efficient Acute Lymphoblastic Leukemia Classification

Nada Jabbar Dubai [a,1], Ola Najah Kadhim [b,2], Fallah H. Najjar [c,d,3,*]

[a] Department of Health Administration Techniques, Technical Institute of Al-Diwaniyah, Al-Furat Al-Awsat Technical University, 58001 Al-Qadisiyah, Iraq
[b] Department of Medical Instruments Techniques, Technical Institute of Al-Mussaib, Al-Furat Al-Awsat Technical University, 51006 Babil, Iraq
[c] Department of Computer Networks and Software Techniques, Technical Institute of Najaf, Al-Furat Al-Awsat Technical University, 54001 Najaf, Iraq
[d] Faculty Department of Emergent Computing, Faculty of Computing, Universiti Teknologi Malaysia, 81310 UTM Johor Bahru, Johor, Malaysia
[1] nada.jabbar.idi@atu.edu.iq; [2] ola.najah@atu.edu.iq; [3] fallahnajjar@atu.edu.iq
* Corresponding Author

ARTICLE INFO

Article history
Received February 08, 2025
Revised April 01, 2025
Accepted April 29, 2025

Keywords
Acute Lymphoblastic Leukemia;
MCB-HyperNet;
Morphological Context Blocks;
ALL;
Leukemia Classification

ABSTRACT

Acute Lymphoblastic Leukemia (ALL) is an aggressive hematologic malignancy that necessitates early and accurate diagnosis for improved therapeutic efficacy. Although it is a routine practice, the visual blood smear analysis is tedious and subject to human inaccuracies. This paper proposes a novel morphology-guided deep learning approach called Morphological Context Blocks (MCB)-HyperNet embedding morphological operations into a hybrid CNN architecture. The CNN architectures depend mainly on automatic learning through convolutive filters, so they miss crucial morphological features that distinguish between leukemic and normal cells. In this study, we propose a deep learning-based approach that directly incorporates morphological dilation and erosion in the deep learning data pipeline to exploit the potential of morphological feature extraction for our specific task, resulting in enhanced accuracy and reduced diagnostic costs, which ultimately can improve patient outcomes. In addition, the computational efficiency and modularity of the MCB-HyperNet framework facilitate easy adaptation and scalability to many other medical imaging tasks, such as the classification of various diseases, except the classification of leukemia. We trained the proposed MCB-HyperNet on different image resolutions from the ALL dataset (168×168, 224×224, 256×256), different batch sizes (16 and 32), and also different training epochs (30, 35, 40, 45, 50) to get the best hyperparameter configuration. The MCB-HyperNet takes advantage of the strong feature extraction ability of ResNet and the light computing resource of MobileNetV3, ultimately obtaining 99.69% accuracy, 98.78% precision, 99.49% sensitivity, 99.12% F1-score, and 99.78% specificity. This new integration greatly enhances the accuracy of early detection, minimizes diagnostic errors, and could have significant clinical and economic advantages. MCB-HyperNet is a mini CNN, so it shows a good balance between efficiency and accuracy, making scalability and extensibility possible in more medical imaging tasks.

1. Introduction

Acute Lymphoblastic Leukemia (ALL) is an aggressive hematological malignancy most seen in children, necessitating both timely and accurate diagnosis to improve survival [1]-[5]. Diagnosing ALL is the classical procedure of microscopic lymphocyte blood smear images in which human experts check lymphocyte cell morphology and compare it with normal cells [6], [7]. In contrast, this process is time-consuming, human error-driven, and reliant upon the expertise of hematologists [8], [9]. The emergence of digital pathology and medical imaging Artificial Intelligence (AI) has opened applications for automated diagnostic models, significantly improving the efficiency and accuracy of diagnosing leukemia [10]-[12]. Deep learning, particularly Convolutional Neural Networks (CNNs), has achieved convincing performance in classifying blood smear images [13]-[15].

Nevertheless, traditional CNN-based architectures mainly depend on learning features using convolutional filters [16], [17]. In contrast, important structural and morphological features essential for distinguishing leukemic from normal cells are often neglected [18], [19]. In hematopathology, the analysis of morphology is an important step that enables the recognition of unique features, including cell size, shape, nuclear configuration, and margin contours [20], [21]. Classical image processing techniques like mathematical morphology implement dilation and erosion operations to boost the edges and identify abnormal cell structures [22]-[24]. Although effective, these operations have not been directly incorporated into deep learning models so far, restricting the capacity of CNN for maintaining fine morphological features. Deep learning-based methods for leukemia classification, like ResNet, VGG, and MobileNet, have shown strong performance [6], [13], [25]. However, they often fail to generalize across different blood smear samples, particularly with high intra-class variability in cell morphology. This is a limitation, as the state-of-the-art CNN-based classification methods are not robust in a few cases. This establishes the need for a model to help represent morphology by directly enforcing morphology informed priorities within the deep learning framework.

However, to overcome such limitations, we present a Morphology-Guided Deep Learning Framework of ALL classification, which exploits Morphological Context Blocks into a hybrid CNN pipeline. Instead of being merely dependent on learned convolutional filters, our proposed model incorporates morphological operations, specifically dilation and erosion, deeper into the network structure for learning edge-based and shape-based features. ResNet is employed to mine deep hierarchically sparse features, while MobileNetV2 is utilized to efficiently mobilize memory bandwidths, maintaining the required high accuracy in a possibly least computationally weighted manner. The design of MCB-HyperNet is a new module with dilation expanding the bright area, erosion shrinking the dark area, and the morphological gradients focusing on the edges. In addition, incorporating a gating mechanism to the MCB-HyperNet enables it to adaptively determine the importance of different morphological features, allowing only the most relevant structural information to contribute to the classification process.

Moreover, to address this gap, we propose MCB-HyperNet to directly embed a morphological feature learning mechanism in a deep network to improve classification performance without significantly compromising computational efficiency. As far as we know, this study is among the first to seamlessly incorporate mathematical morphology into the deep learning framework for BM image analysis, thus providing an effort to contribute towards AI-powered hematopathology. Such work has substantially contributed to a new landscape in AI-based leukemia classification by incorporating morphological priors into a CNN, providing greater accuracy, robustness, and interpretability. This work forms the basis for future morphology-aware medical AI models that could enable precise disease recognition in a range of medical imaging scenarios by linking the concepts of mathematical morphology to deep learning.

Furthermore, Our contributions are summarized as follows: (i) A novel MCB-HyperNet architecture integrating morphological operations (dilation and erosion) within the CNN framework. (ii) A ResNet is used for deep hierarchical feature extractors, and MobileNetV3 is used for

computational efficiency in a hybrid implementation. (iii) Resulting unprecedented performance metrics with 99.69% accuracy, outperforming all current state-of-the-art methods.

However, the inclusion of morphological operations comes with challenges and risks. The expanded number of morphological modules increases model complexity and can present an overfitting risk for training on smaller or less diverse datasets. In addition, pooling-based approximations of morphological dilation and erosion may also introduce artifacts or inaccuracies, potentially impeding the identification of subtle morphologies important for accurately classifying leukemia subtypes. Moreover, the generalization of such morphology-guided models to other clinical settings, where staining protocols, image resolutions, or slide preparations may differ, is a critical and still open question that has a bearing on their clinical applicability.

Our study balances the trade-off between rate and performance by identifying these challenges. It shows that the MCB-HyperNet framework reaches a state-of-the-art accuracy while guaranteeing acceptable computational efficiency for real clinical applications. However, rigorous hyperparameter tuning and deliberate data augmentation procedures are implemented, to some extent improving the ability of the model to generalize and mitigating the aforementioned inherent shortcomings of the model.

2. Related Works

Deep learning and computational intelligence-based approaches for leukemia classification and detection, which have completely revolutionized the field of medical diagnostics, have become a hot research area [26]-[28]. Artificial intelligence and deep learning improvements made scientists create automated systems that greatly enhance classification performance [29]-[31]. All while minimizing the use of human participants. Leukemia is one of the various types of cancer; their early diagnosis can be lifesaving, especially in the case of ALL [12]. Conventional diagnostics, including blood smear examination and bone marrow aspirates, are labor-intensive, time-consuming, and subject to human errors [7], [12]. Consequently, computational models that utilize machine learning and deep learning algorithms have received considerable interest as they can be used to automate the detection process, improve accuracy, and reduce time to diagnosis [32]. Deep learning is one of the best approaches to leukemia classification, where blood smear images have been used for feature extraction using CNN and transfer learning [33], [34]. Pretrained CNNs have been used in some studies and achieved high classification accuracies [35]. Gokulkrishnan et al. [36] proposed ResNet-50 and ResNet-101 for ALL detection with blood smear images to classify the benign and malignant cells. Their system attained more than 98% precision, indicating the power of profound learning classifiers in exceptional hematology. Similarly, Kadhim et al. [37] Classifying AML via a multi-layer CNN architecture reported accuracies greater than 98% with enormous specificity and sensitivity, establishing the robustness of CNN architectures for distinguishing leukemic cells. Mohamed et al. [38] conducted a study in which a deep learning model was created to classify eight blood cancer types, including subtypes of AML and ALL. The performance of VGG16 and DenseNet-121 was compared, and the authors concluded that VGG16 gave the highest classification accuracy at 98.2%.

Furthermore, Rejula et al. [39] presented a modified Adaptive Neuro-Fuzzy Inference System (ANFIS) model that combines neural networks and fuzzy logic to classify leukemia. It had high sensitivity and specificity and addressed some of the limitations of traditional classification. Feature optimization has been a critical component in minimizing computation costs without sacrificing classification accuracy for leukemia detection. Once again, choosing dependent and independent variables plays a huge role in making the model more efficient by eliminating redundancy and improving interpretability. Metaheuristic algorithms have been integrated into these research studies to select features and show better performance. Awais et al. [40] presented a nature-based optimization approach (deep-feature optimization) using the binary Grey Wolf Algorithm, with classification accuracy for ALL subtypes being 98.14%. Their approach reduced the feature vector size by 80%, keeping the important discriminative information but lessening the computational complexity. Another study by Awais et al. [41] proposed a new memetic deep feature optimization method

composed of a neural ensemble and a binary whale optimization algorithm. The computational model achieved a total accuracy of 99.15%, indicating the high classification potential, accompanied by an impressive reduction in feature vector size at 85%. The feature selection techniques demonstrate more accelerated convergence properties than classical optimization methods, allowing for their direct application in real-time leukemia detection systems.

Most deep learning models are challenging to replicate, mainly due to their computational cost, which reminded researchers to investigate lightweight architectures to classify leukemia whilst maintaining their robustness. Batool and Byun [42] proposed an EfficientNet-B3-based model integrated with a depthwise separable convolutional block to improve classification performance and reduce the model size. Their lightweight deep learning model proved to be significantly efficient in detecting leukemia and suitable for practical applications in clinical settings, particularly in resource-limited areas. Lalithkumar et al. [43] proposed a hybrid model that combines the Capsule Networks (CapsNet) elements and generalizes the improvement in classification accuracy while finding the balance between classification accuracy and interpretability. CapsNet's retention of spatial relationships in image data makes it especially useful for differentiating among leukemia subtypes. Ultra-light models are optimized for minimal memory footprint and computation time, making them a natural fit for deployment on mobile or edge-computing hardware where computation is a premium. Many researchers have adopted transfer learning for detecting leukemia, tuning their CNNs that have been pre-trained for extracting features followed by a classification module. Acquiring large, labeled datasets for leukemia detection can be problematic, so transfer learning allows models to be fine-tuned from large image datasets to classify various leukemia types. Preanto et al. [44] Next, multiple pre-trained CNNs like InceptionV3, ResNet101, VGG19, DenseNet121, and MobileNetV2 were used for feature extraction. They achieved an accuracy of 87% as well after using feature selection techniques, including ANOVA, Recursive Feature Elimination (RFE), and Principal Component Analysis (PCA) to help classify the data. Their work emphasizes the importance of transfer learning to improve classification accuracy with small training databases. In addition, Tusar et al. [45] proposed an intelligent telediagnosis system for ALL detection using histopathological deep learning. Their model helps to facilitate remote diagnosis and telemedicine, as hematologists are not always available to those patients. This not-vein approach highlights the growing utilization of deep learning in remote healthcare and has implications for improving leukemia detection in underserved areas.

Another promising approach is hybrid learning and ensemble models, which often involve combining several models to improve overall accuracy for leukemia classification. Rejula et al. [39] proposed, based on ANFIS, that combined neural networks and fuzzy logic and got 97.14% accuracy. The novel solution they proposed combined the advantages of both techniques and demonstrated efficacy in overcoming certain limitations of single-model classifiers. Similarly, Awais et al. [41] proposed an ensemble-based model that integrates GoogleNet CNN and 88-layer deep CNN, which could achieve state-of-the-art accuracy on B-ALL subtype classification at 98.69%. Their studies introduce an ensemble learning approach that considers multiple classifiers and addresses issues related to imbalanced datasets, which enhance robustness and ultimately allow for greater efficacy in real-world leukemia diagnosis. This showcases the hybrid potential outcome of fulfilling the reliability and generalization problem in classification. Tusar et al. [46] proposed an ALL subtype detection system, for which the authors employed deep neural networks (DNNs) classifiers to classify leukemia cells with an accuracy of 96.13%. Atteia et al. [47] introduced a hybrid feature-learning model utilizing Particle Swarm Optimization (PSO) in conjunction with PCA for blood cancer classification, resulting in a 97.4% accuracy. Rehman et al. [25] Deep learning-based segmentation methods for ALL detection, achieving 97.78% accuracy due to the high performance of CNN-based classification models. However, based on previous research, the morphology-guided deep learning method we proposed in this work characterized a new feature design of the structures corresponding to the data for CNN by introducing MCB. Although convolutional filters would explicitly teach convolutional models, this inherently applies morphological operations (dilate and erode), raising edge and deduction researchers for blood smear images.

3. Methodology

This study presents the MCB-HyperNet Deep Learning Framework for ALL classification with MCB in a hybrid ResNet and MobileNetV3 architecture.

3.1. Dataset Description

The ALL dataset comprises 3,256 Peripheral Blood Smear images from 89 patients [48], [49]. The images were labeled in four classes: Benign, Early Pre-B, Pre-B, and Pro-B. The data was split into training, validation and testing parts (80%, 10%, and 10%, respectively). Fig. 1 Displays sample images from the ALL dataset. Nevertheless, we believe the dataset will be useful for training our proposed models for automated diagnosis to classify the dataset.

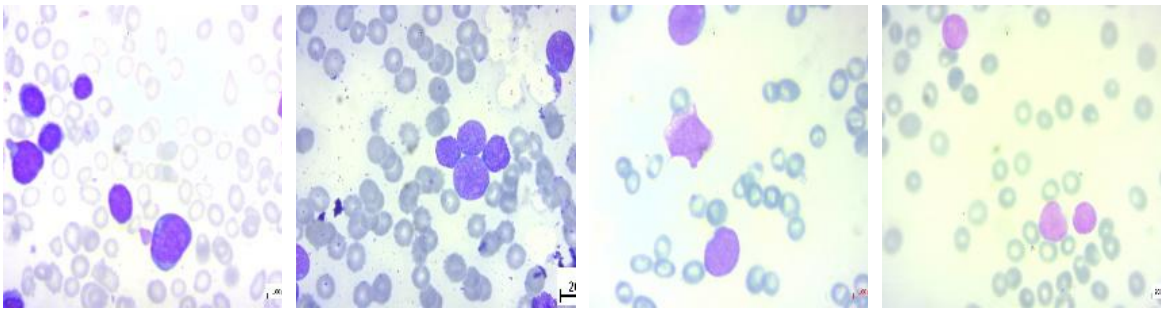

Fig. 1. Sample images, from left to right, Benign, Early Pre-B, Pre-B and Pro-B [48], [49]

Next, we will provide a complete view of how our proposed MCB-HyperNet extract feature works.

3.2. Feature Extraction, Morphological Operations, and Model Architecture

In this subsection, we will go through the MCB-HyperNet computational flow step by step. The MCB-HyperNet stage transforms the input feature maps by applying conventional operations, morphological operations, pooling, and fusion mechanisms.

At the beginning, the input image (im) has the shape of:

$$im \in \mathbb{R}^{H,W,C} \tag{1}$$

Where H, W, C denote the height, width, and number of channels, which are 3 channels, respectively. The image pixels are normalized between zero and one.

The ResNet block represents the first stage of MCB-HyperNet. ResNet is used to extract hierarchical, deep-level sparse features using (2).

$$\mathcal{F}_{res} = \sigma\left(BN\left(W_2 * \sigma\left(BN(W_1 * im + b_1)\right) + b_2\right)\right) + im \tag{2}$$

Where W_1, W_2 denote to the trainable kernels (3×3 filters), b_1, b_2 denote the bias terms, BN denote the Batch Normalization, and $\sigma(.)$ denote the Rectivaed Learning Unit (ReLU) activation function of channels, respectively. The output of ResNet at this stage remains the same spatial size H, W but has more feature channels.

$$\mathcal{F}_{res} \in \mathbb{R}^{H,W,64} \tag{3}$$

The proposed MCB-HyperNet improves feature extraction using morphological operations (dilation and erosion), which are approximated by max and min pooling operations. The Dilation operation is a morphological operation that allows us to permeate the image.

$$\mathfrak{D}1(im) = \max_{(i,j)\in\mathcal{N}(x,y)} im(i,j) \tag{4}$$

Where $im(i,j)$ represents the input feature map, $\mathcal{N}(x,y)$ represents the local neighborhood with (k,k) kernel size, and $\mathfrak{D}1(im)$ represents the output of the dilated operation.

The dilation operation can be implemented through deep learning utilizing MaxPooling with a stride of 1.

$$\mathfrak{D}1(\mathcal{F}_{res}) = MaxPool2D(\mathcal{F}_{res}, PoolSize = k, Stride = 1, Padding = \text{same}) \quad (5)$$

Conversely, erosion $\mathcal{E}1(im)$ is the opposite operation that reduces the bright spots and increases the dark areas. It is calculated via min pooling that negative MaxPooling can approximate.

$$\mathcal{E}1(im) = \min_{(i,j)\in\mathcal{N}(x,y)} im(i,j) \quad (6)$$

Since deep learning does not have min pooling, we approximate it using negative MaxPooling.

$$\mathcal{E}1(\mathcal{F}_{res}) = MaxPool2D(-\mathcal{F}_{res}, PoolSize = k, Stride = 1, Padding = same) \quad (7)$$

The gradient $\mathcal{F}_{MCB1}$ that highlights the edges is calculated as follows:

$$\mathcal{F}_{MCB1} = \mathfrak{D}1(\mathcal{F}_{res}) - \mathcal{E}1(\mathcal{F}_{res}) \quad (8)$$

The gradient output at this stage remains the same spatial size H, W but has more feature channels.

$$\mathcal{F}_{MCB1} \in \mathbb{R}^{H,W,64} \quad (9)$$

Furthermore, we integrate MobileNetV3, a lightweight CNN that down samples the image while extracting meaningful features. MobileNetV3 is used to refine the extracted features using depthwise separable convolutions utilizing 10 to 13.

$$\mathcal{F}_{DW} = DepthWiseConv2D(\mathfrak{D}_{MCB1}, W_{dw}) \quad (10)$$

$$\mathcal{F}_{PW} = PointWiseConv2D(\mathcal{F}_{DW}, W_{pw}) \quad (11)$$

$$\mathcal{F}_{SE} = SE(\mathcal{F}_{PW}) \quad (12)$$

$$\mathcal{F}_{mob} = \sigma(\mathcal{F}_{SE}) \quad (13)$$

Where W_{dw} represents the input feature map, W_{dw} represents the local neighborhood with (k,k) kernel size, and $SE(.)$ represents the output of the dilated operation. The dilation operation can be implemented through deep learning utilizing MaxPooling with a stride of 1.

The gradient output at this stage reduces the resolutions H, W into H_d, W_d.

$$\mathcal{F}_{mob} \in \mathbb{R}^{H_d,W_d,576} \quad (14)$$

Where $H_d = W_d = 6$ for input 168×168 and $H_d = W_d = 8$ for input 244×244 and 256×256.

The dilation operation can be implemented through deep learning utilizing MaxPooling with a stride of 1.

$$\mathfrak{D}2(\mathcal{F}_{mob}) = MaxPool2D(\mathcal{F}_{mob}, PoolSize = k, Stride = 1, Padding = \text{same}) \quad (15)$$

Since deep learning does not have min pooling, we approximate it using negative MaxPooling.

$$\mathcal{E}2(\mathcal{F}_{mob}) = MaxPool2D(-\mathcal{F}_{mob}, PoolSize = k, Stride = 1, Padding = \text{same}) \quad (16)$$

The gradient $\mathcal{F}_{MCB2}$ that highlights the edges is calculated as follows:

$$\mathcal{F}_{MCB2} = \mathfrak{D}2(\mathcal{F}_{mob}) - \mathcal{E}2(\mathcal{F}_{mob}) \quad (17)$$

The gradient $\mathcal{F}_{MCB2}$ output at this stage remains the same spatial size H_d, W_d.

$$\mathcal{F}_{MCB2} \in \mathbb{R}^{H_d, W_d, 576} \tag{18}$$

We apply the MaxPooling in order to align the $\mathcal{F}_{res}$ and $\mathcal{F}_{MCB1}$ feature maps with $\mathcal{F}_{mob}$ and $\mathcal{F}_{MCB2}$.

$$\mathcal{F}_{res\_d} = MaxPool2D(\mathcal{F}_{res}, PoolSize = (H/H_d, W/W_d)) \tag{19}$$

$$\mathcal{F}_{MCB1\_d} = MaxPool2D(\mathcal{F}_{MCB1}, PoolSize = (H/H_d, W/W_d)) \tag{20}$$

Once all the features are aligned, we connect them using (21).

$$\mathcal{F} = concat(\mathcal{F}_{res\_d}, \mathcal{F}_{MCB1\_d}, \mathcal{F}_{mob}, \mathcal{F}_{MCB2}) \tag{21}$$

All feature maps at this stage have:

$$\mathcal{F} \in \mathbb{R}^{H_d, W_d, 1280} \tag{22}$$

Finally, A fully connected (FC) layer and a SoftMax classifier predict the ALL subtype using the probability distribution over the classes $\mathcal{P}(y)$ [50].

$$\mathcal{P}(y) = \text{concat}(W\mathcal{F} + b) \tag{23}$$

This framework explicitly extracts morphological features that conventional CNNs, such as cell boundaries, nuclear texture and edge details, may not maintain. Fig. 2 displays the methodology for ALL disease classification.

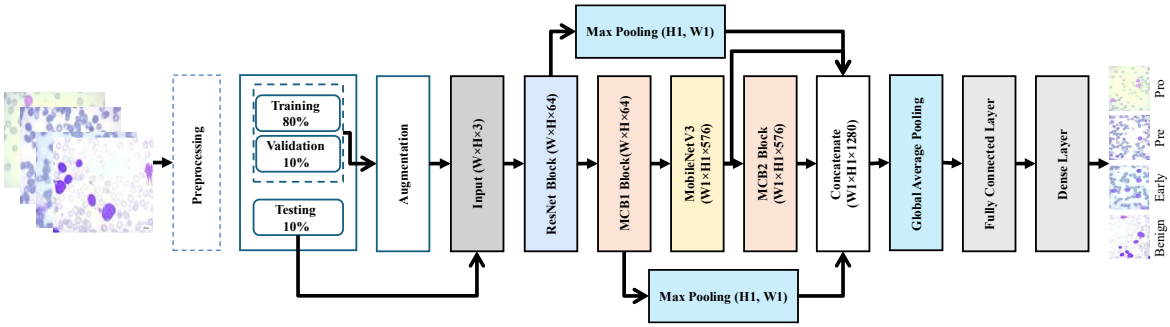

Fig. 2. Methodology for ALL classification

Furthermore, Fig. 3 illustrates the proposed CMB-HyperNet.

3.3. Scalability and Potential Pitfalls

Scalability, especially concerning resource-constrained clinical settings, needs thorough consideration. Despite powerful computing efficiency from leveraging MobileNetV3, MCB-HyperNet is still more demanding than simpler architectures dedicated to deployment in very resource-constrained scenarios like mobile or edge-computing devices. Thus, future works should thoroughly compare multilayered approaches with lighter-weight architecture or other hybrid models to analyze performance vs resource usage trade-offs and real-world deployability. Another important consideration is how well the model will generalize to the variability seen in real-world data. This is because blood smear images in clinical practice have common staining inconsistencies, illumination variation, and imaging artifacts, potentially hindering morphological feature extraction accuracy. Even so, while data augmentation methods used in this paper, including random rotations, flips, and changing the brightness/contrast and other factors, alleviate this problem to some extent, the inherent challenges that arise with this limited and very variable, uncontrolled clinical datasets remain. Hence, the empirical robustness and generalization ability of MCB-HyperNet still rely on the proper data curation and the right augmentation strategies. Moreover, hybridizing ResNet and MobileNetV3 architectures with MCB in a CNN layer introduces complexity trade-offs for the models. This shows

the ability to compensate different aspects of building a model (dimensional feature extraction quality (ResNet), computational resource efficiency (MobileNetV3)) but, after all, this can be a sign of increasing the complexity of the model and adding a factor of problems with overfitting, especially on lower dimensional or unbalanced datasets. While extensive hyperparameter tuning and validation offer some assurance against this concern, robust empirical nuance on larger multi-center datasets would be critical to determining our approach's scalability and generalization boundaries.

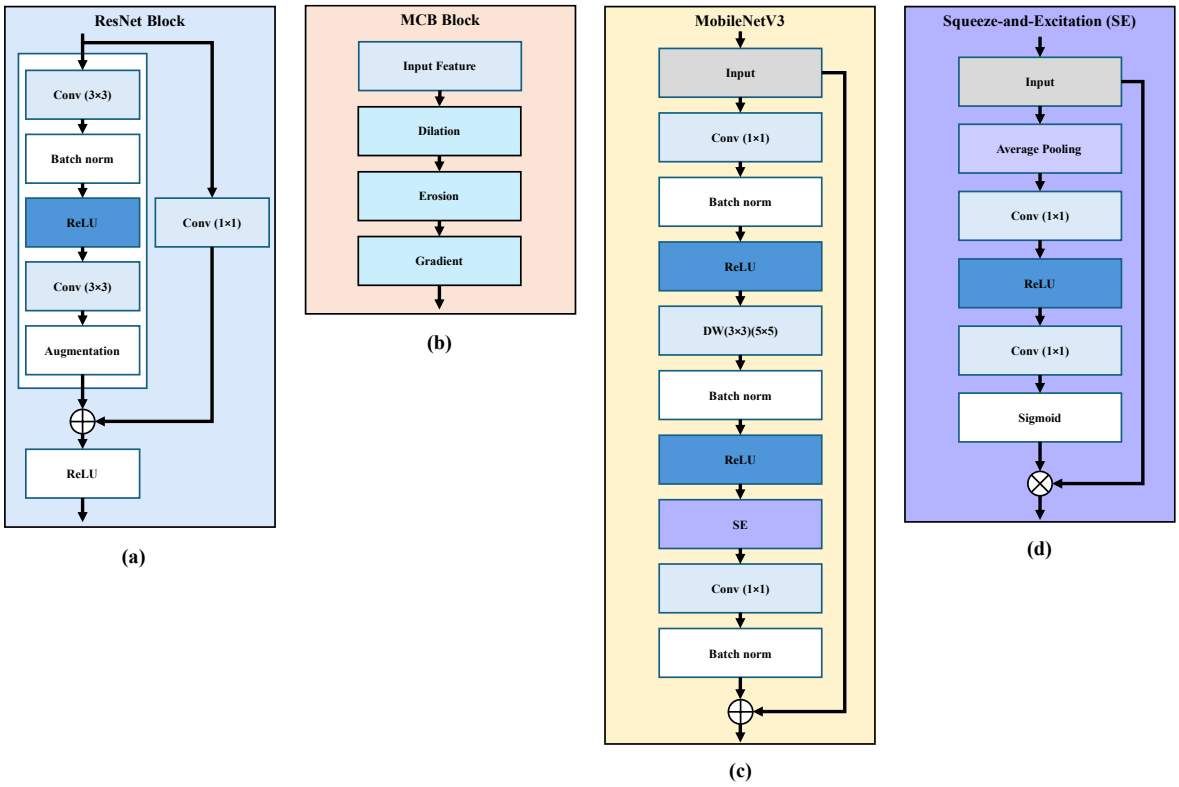

Fig. 3. The proposed MCB-HyperNet Blocks (a) ResNet Block, (b) MCB (1, 2) Blocks, (c) MobileNetV3 Block, and (d) Squeeze and Excitation (SE) Block

4. Proposed Method

In order to find the optimal hyperparameter configuration, we trained the proposed MCB-HyperNet on various image resolutions, batch size and training epochs using the ALL dataset. The ALL dataset is divided into training, validation, and testing 80:10:10. The data treatment aimed to optimize classification performance accuracy, precision, sensitivity (recall), F1-score, and specificity.

4.1. MCB-HyperNet Performance Evaluation

To examine the influence of diverse hyperparameters, we assessed performance based on different image resolutions (168×168, 224×224, 256×256), different batch sizes (16 and 32), and also different training epochs (30, 35, 40, 45, 50). Performance was evaluated using accuracy, precision, recall (sensitivity), F1-score, and specificity. Multiple data augmentation methods are applied to the input images before training MCB-HyperNet to augment its generalization ability and reduce overfitting. Since blood smear images may have differences in color intensity, illumination and angle, augmentation also guarantees that the model extracts robust and invariant features. The augmentation methods used are random rotations (±15°) to reflect the varying orientations of blood smear, horizontal and vertical flipping to enhance dataset diversity, and changes of brightness and contrast to accommodate variations in staining intensity among different samples.

Moreover, image rescaling, which normalizes pixel values from [0, 255] to [0, 1], is performed to ensure that the dataset complies. These transformations are applied during training, enabling the

model to observe variations of the identical samples and consequently enhancing its capacity to generalize to unseen data. Examples of augmented images used during training are shown in Fig. 4.

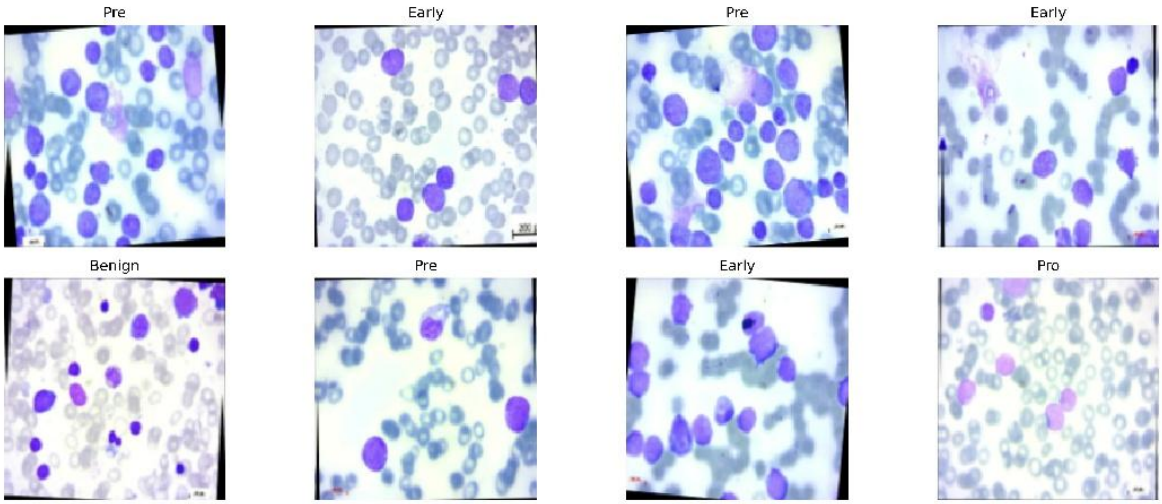

Fig. 4. Augmented images used in training

We analyzed the impact of different hyperparameters on classification performance. Furthermore, the experimental results offer insight into the effects of distinct values for hyperparameters, namely image resolution, batch size, and epochs of training in the behavior of the MCB-HyperNet model when making the classification of leukemia. However, each performance metric trends differently based on those, as illustrated in Fig. 5, Fig. 6, Fig. 7, Fig. 8, Fig. 9.

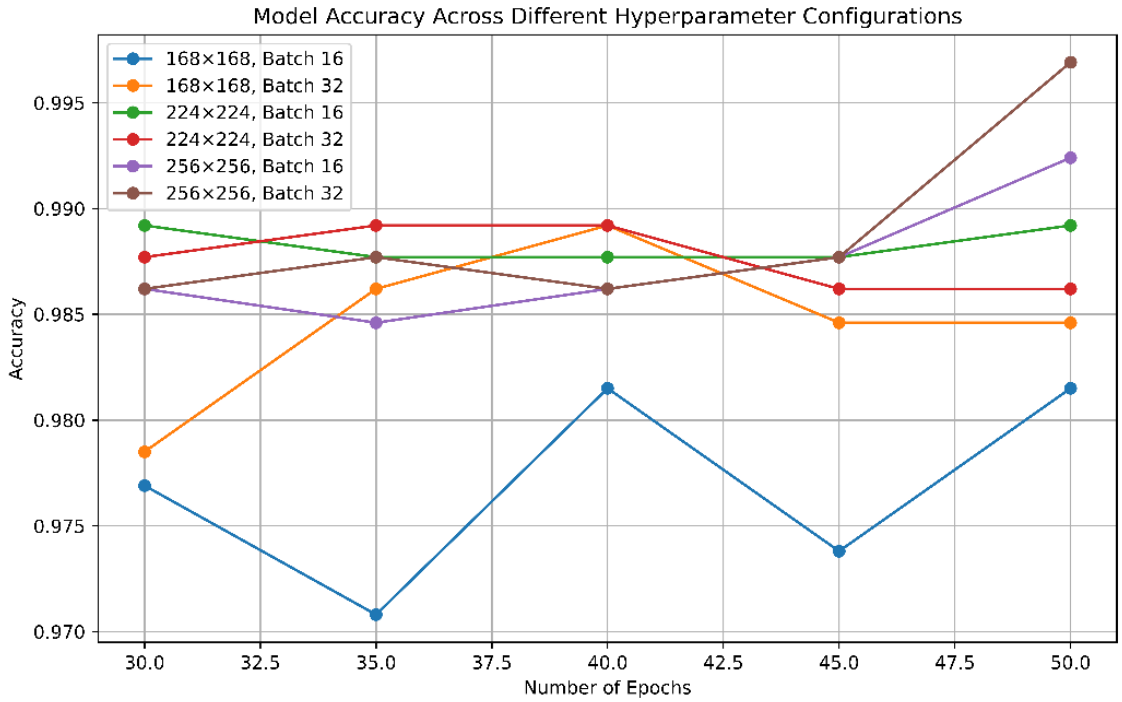

Fig. 5. Model accuracy across different hyperparameter configurations

The trend across epochs in terms of accuracy indicates that as we move towards more training epochs, our classification performance tends to increase, which is expected. The best accuracy of 99.69% was achieved on the image resolution of 256×256, the batch size 32, and 50 epochs. The accuracy decreased for the lower resolutions (168×168), illustrating that the image's details improve the model's learning. A larger batch size (32) consistently outperformed even batch size 16, implying

that larger batch sizes help in better generalization. We noticed that with a greater number of epochs, the accuracy of the networks improved progressively; however, some fluctuations were observed, especially in the lower-resolution images.

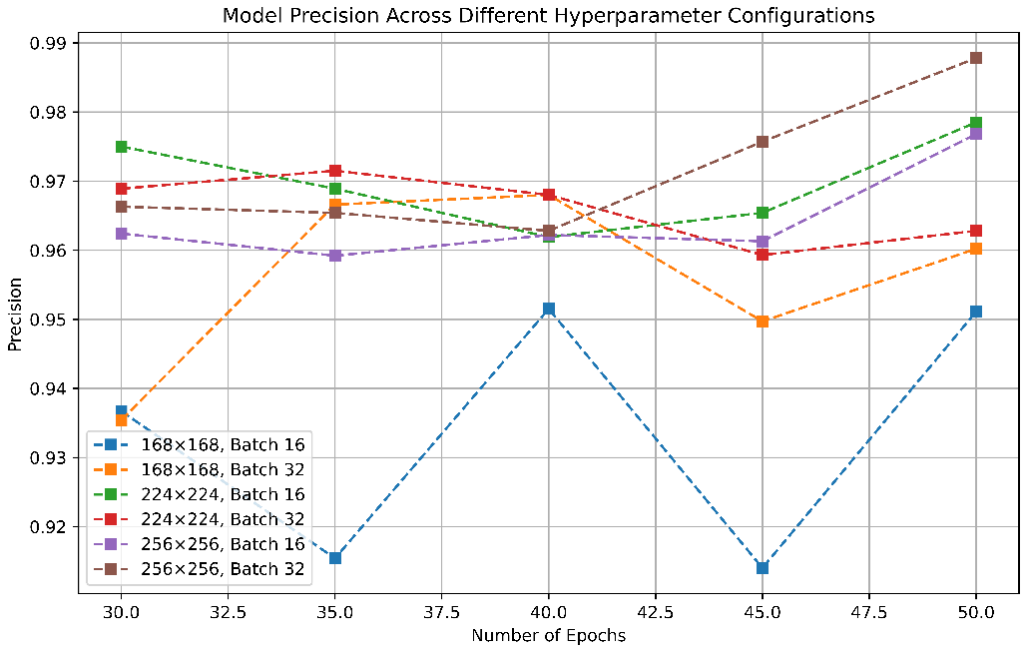

Fig. 6. Model precision across different hyperparameter configurations

Precision, which measures the model's ability to classify positive cases correctly, exhibited a similar pattern concerning accuracy. The maximum precision of 98.78 is obtained by 256×256 resolution, 32 batch sizes, and 50 epochs. Precision was consistent across all configurations, although batch size 32 usually performed better than batch size 32. This suggests that epoch learning is more in-depth and that feature extraction is better due to the smaller batch size. In addition, precision is of utmost importance in medical diagnosis, focusing on minimizing false positives, and these results strongly indicate this model's utility.

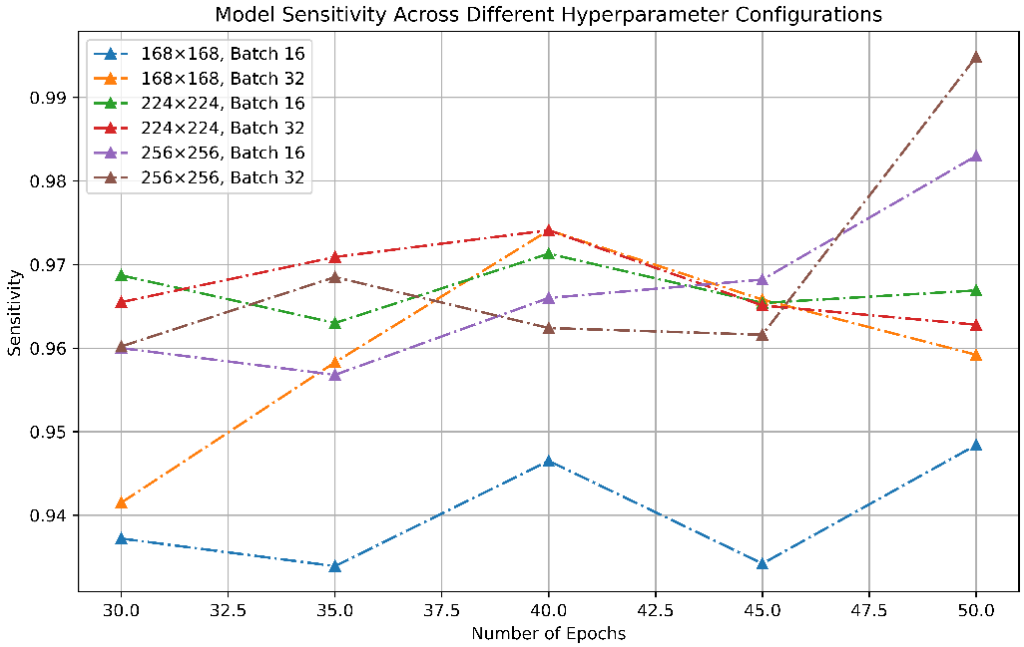

Fig. 7. Model sensitivity across different hyperparameter configurations

Sensitivity (recall), which quantifies the model's ability to detect true positive cases, was better for cases with higher image resolution and longer training. The highest recall value of 99.49% was achieved using 256×256 resolution, batch size 32, and 50 epochs. We found that lower resolutions (168×168) diminished sensitivity, likely owing to loss of critical image detail. Because recall is critical in medical applications where failure to identify a positive case can be injurious, these findings validate that the model can correctly identify more leukemia-positive cases with more training epochs and resolution.

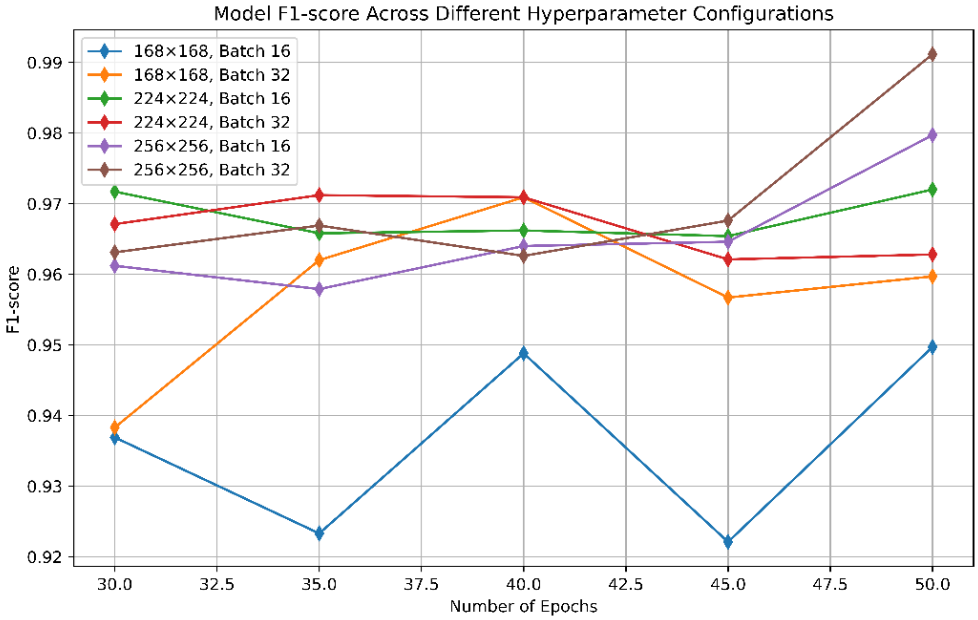

Fig. 8. Model F1 score across different hyperparameter configurations

Similar to the overall trend with improved resolutions and longer training, the F1-score, which combines precision and recall, also improved. An F1 score of 99.12% was achieved at resolution 256×256, batch size 32, and 50 epochs. This metric guarantees that false positives and false negatives are both reduced. The replicated F1 scores across different epoch configurations indicate that the model is well-optimized, with no major signs of overfitting.

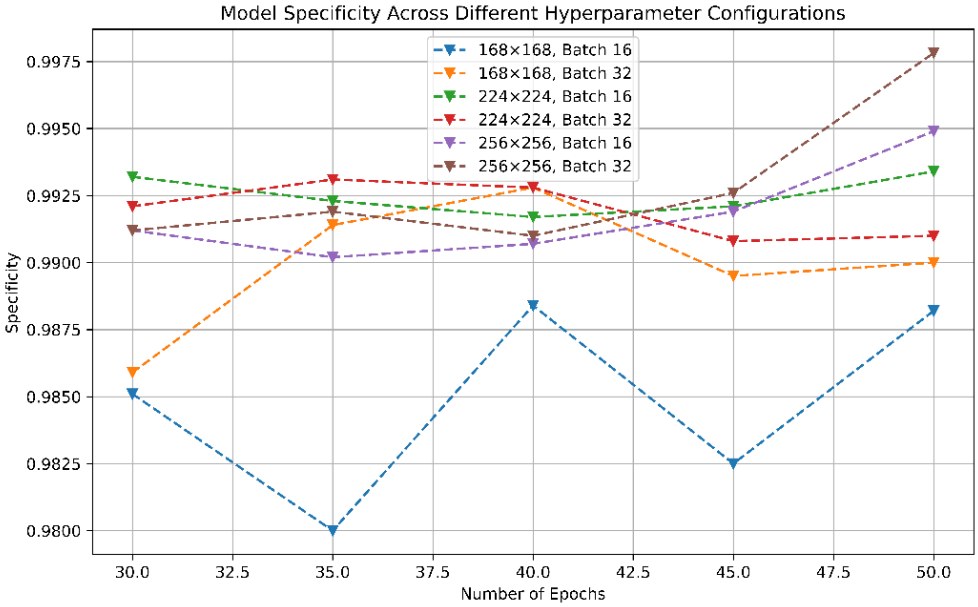

Fig. 9. Model specificity across different hyperparameter configurations

Furthermore, specificity, which measures the model's ability to identify negative cases accurately, progressively improves with higher resolutions and additional training. The highest specificity, 99.78%, was achieved with the same best-performing configuration, including resolution 256×256, batch size 32, and epochs 50. These high specificity values show that the model can minimize false positives, a crucial aspect of medical diagnosis where false alarms can lead to undue anxiety and unwarranted treatments for patients.

4.2. Comparison with Relevant Literature

In this subsection, we present experimental results to evaluate the performance of our model. We evaluate classification accuracy over multiple metrics, such as the confusion matrix, that give us insights into class-wise performance and misclassification. We also look at misclassified samples to identify patterns of errors and possible difficulties encountered by the model. Fig. 10 presents the training and validation accuracy and loss over 50 epochs.

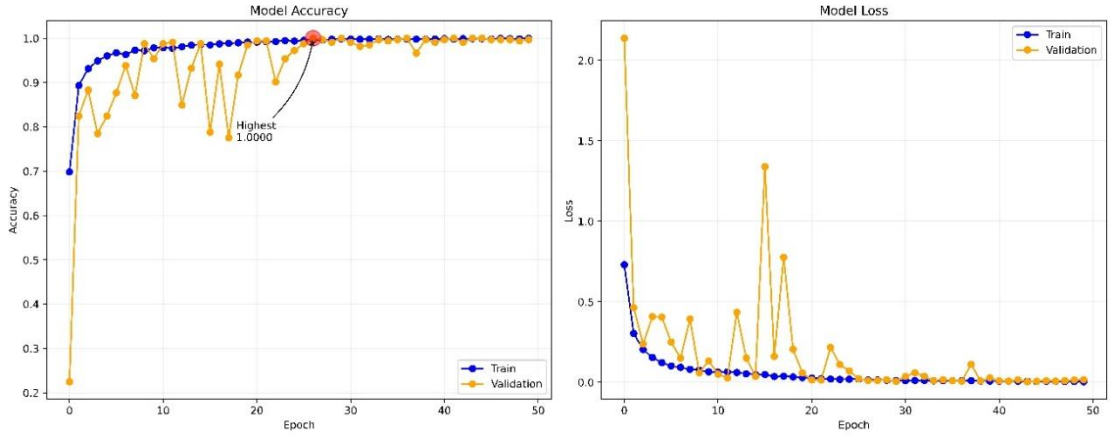

Fig. 10. MCB-HyperNet monitoring accuracy and loss during

Our access for 50 epochs shows the training, validation accuracy, and loss graphs. The accuracy plot further shows that with the training loss decreasing close to 0 in the beginning epoch, the training accuracy increases rapidly and stabilizes at around 15 epochs with 100% accuracy. Validation accuracy shows a similar trend but can be erratic in the early epochs before converging around 100%. The model achieves the highest validation accuracy of 1.0000, meaning it correctly classifies all validation samples at some epochs.

We can further affirm this fact with the loss plot. Steady training gradually smoothens and consistently indicates that the model is learning. In contrast, the validation loss varies widely in the early epoch and stabilizes at a lower value. These variations indicate instability in generalization, which an imbalanced dataset, batch diversity, or a high learning rate in the first few epochs can cause. Although some individual spikes of increases in validation loss can be correlated to instances where the model thinks it has classified an image one way, this trend indicates that if the process is left on, eventually, the model finds a strong decision boundary. MCB-HyperNet test set confusion matrix. Fig. 11 shows the proposed MCB-HyperNet test set confusion matrix. Diagonal values represent correctly classified samples, while the off-diagonal values represent misclassifications.

The model has high classification performance, with only two misclassifications in 325 samples. Exploring feature importance and further dataset augmentation might allow for this domain to be tuned so we can accurately predict it. Fig. 12 displays the two misclassified samples.

The precision and recall for Early, Pre, and Pro classes are perfect, 100%, while there is still some confusion between the Benign and Early classes, and small improvements can be made to reduce this. Finally, Table 1 displays the comparative results of our model against baseline approaches.

As shown in Table 1, the comparative matrices of classification algorithms and accuracy indicate that our proposed MCB-HyperNet model considerably outperforms the previous state-of-the-art

methods regarding accuracy, sensitivity, F1-score, and specificity. Our model results in an accuracy of 99.69%, the best among all the models compared. The closest competitor reported by Awais et al. resulted in 98.69% accuracy, which is 1% worse than our approach. Recent models such as Gokulkrishnan et al. and Kadhim et al. do well, but none outperform the MCB-HyperNet accuracy level. MCB-HyperNet also has a high precision of 98.78%, showing low false positive rates apart from accuracy. However, Atteia et al. demonstrated the highest precision (99.30%).

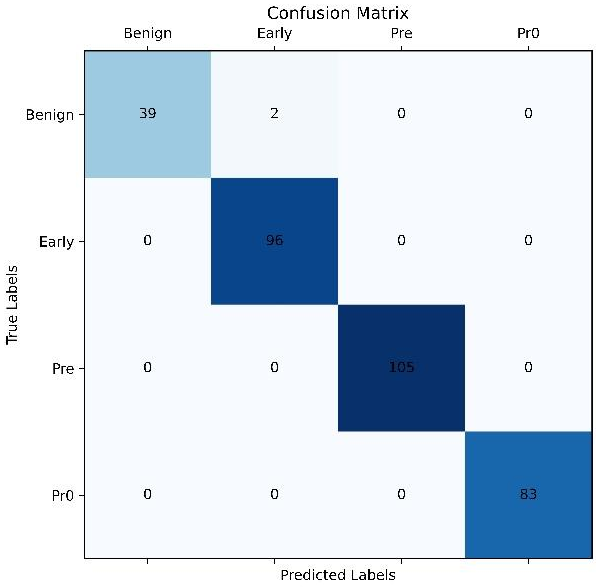

Fig. 11. MCB-HyperNet test set confusion matrix

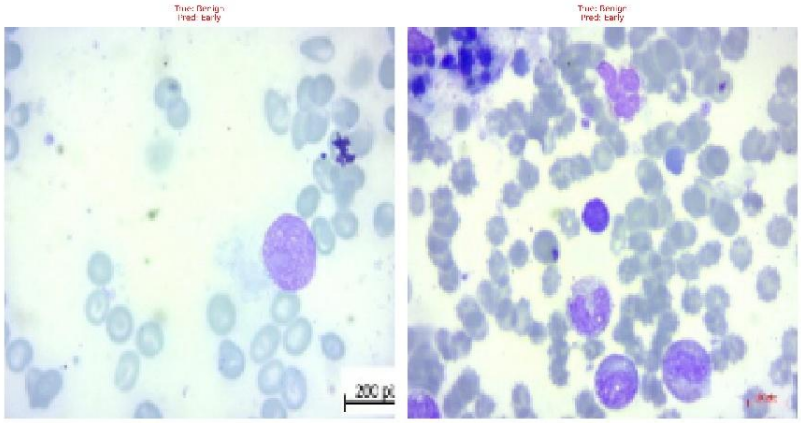

Fig. 12. Misclassified samples

Table 1. Classification performance comparison with relevant literature

Author	Year	Accuracy	Precision	Sensitivity	F1-score	Specificity
Rehman et al. [25]	2019	97.78%	-	-	-	-
Atteia et al. [47]	2023	97.40%	**99.30%**	96.60%	98.93%	-
Gokulkrishnan et al. [36]	2023	98.62%	98.75%	98.5%	98.75%	-
Kadhim et al. [37]	2023	98.15%	96.00%	94.68%	95.24%	98.87%
Batool and Byun [42]	2023	96.81%	97.27%	97.87%	97.57%	
Mohamed et al. [38]	2023	98.10%	-	-	-	-
Awais et al. [40]	2024	98.69%	-	-	-	-
Awais et al. [41]	2024	98.14%	98.14%	98.11%	98.14%	-
Tusar et al. [45]	2024	97.00%	97.00%	96.00%	96.00%	-
Lalithkumar et al. [43]	2024	96.00%	96.88%	96.00%	96.50%	
Our proposed MCB-HyperNet	2025	**99.69%**	98.78%	**99.49%**	**99.12%**	**99.78%**

Nevertheless, their overall performance (97.40%) is lower than our model, indicating that their approach may face difficulty generalizing. In addition, MCB-HyperNet has the best sensitivity of 99.49%, which indicates its ability to detect TP cases while minimizing FN cases. In contrast, Gokulkrishnan et al. reported 98.5% sensitivity, which, though high, was lower than the performance of our model.

MCB-HyperNet achieved the highest F1-score, 99.12%, compared to other approaches, which indicates a better balancing of precision and recall. While Atteia et al. achieved 98.93%, their lower accuracy indicates that their model is less robust than ours. Moreover, our model achieves the highest specificity (99.78%), resulting in very low false positive rates. The only other models that showed specificity were Kadhim et al. at 98.87%, still below our approach. The MCB-HyperNet performs best on all classification evaluation metrics compared with all models. The model obtains significant accuracy, sensitivity, and specificity. However, the precision and F1-score are also high. These improvements showcase the power of our demonstrated methodology and architectural innovations, establishing MCB-HyperNet as the new state-of-the-art classification network.

Finally, The MCB-HyperNet method proposed in this work achieves an impressive accuracy of 99.69%, sensitivity of 99.49%, and specificity of 99.78% performance in ALL classification, surpassing that of the existing best models. Combining morphological operations with a hybrid CNN architecture allows improved classification results to be achieved through the morphological features that traditional convolutional layers would otherwise omit. The in-depth theory behind perfect learning and loss/accuracy curves, along with visual representations of misclassified examples and confusion matrices, only highlight how robust and generalizable the model is with hyper-tuning and additional data showing its promise.

4.3. Limitations

Even though the proposed MCB-HyperNet framework performance is promising, it has some inherent limitations we explicitly recognize. The main methodological limitation is the approximation used to compute morphological operations (dilation and erosion) with pooling operations suitable for deep learning. Firstly, there are issues using negative MaxPooling as an approximation of erosion, such as excess artifacts or loss of fine-scale features. These features are especially important when differentiating the subtle morphological differences between ALL subtypes. While this approximation greatly reduces computation costs and simplifies integration with CNN architectures, it can potentially lose the fine-tuned or more subtle difference in morphological features.

5. Conclusion

In this study, we propose MCB-HyperNet, a new deep learning framework to classify ALL using hybrid CNN architecture exploiting morphological operations. Although conventional approaches based on an ensemble of CNNs heavily depend on learned convolutional filters, our model complements them with morphological priors' dilation and erosion to refine features retaining the shapes and contours necessary for proper leukemia classification. The incorporation of ResNet enables MCB-HyperNet to learn deep hierarchical features while adopting MobileNetV3 optimizes it for computational efficiency, thus ensuring the overall performance is accurate, robust, and interpretable for hematopathological analysis. It was found through well-defined hyperparameter tuning that the best configuration was the image size was 256×256 pixels, the batch size was 32, and the training epoch was 50, where the best performance metrics with an accuracy of 99.69%, a sensitivity of 99.49%, a specificity of 99.78% and a precision of 98.78%. MCB-HyperNet outperforms several state-of-the-art leukemia classification methods.

Moreover, comparing the most recent deep learning models demonstrates MCB-HyperNet's advantage over them concerning classification performance and reliability. The present study forms part of a novel approach to AI-powered hematopathology by bridging start-of-the-art image processing methods and contemporary deep learning tools by wrapping the morphological operations in the deep learning pipeline. Morphology-aware features increase the model's generalization potential

on varied blood smear samples, decreasing errors and improving clinical applicability. This work builds upon the use of morphology-guided AI in medical imaging. It demonstrates shape-based potential that can be generalized to other aspects of hematological imaging and pathologies that other models can address. MCB-HyperNet also shows competitive performance in ALL classification, generalization and deployment ability, which remains challenging. Future research efforts should scale datasets, improve the efficiency of models, and strengthen clinical integration. With the restructuring of AI development in this area, morphology-guided deep learning could transform AI-powered hematopathology and enable worldwide to be more accurate, accessible, and automated leukemia diagnostics.

Author Contribution: All authors contributed equally to the main contributor to this paper. All authors read and approved the final paper.

Funding: This research received no external funding.

Conflicts of Interest: The authors declare no conflict of interest.

References

[1] A. Ferraz, S. Faria, M. Jerónimo, and M. G. Pereira, "Parental psychological adjustment in pediatric acute lymphoblastic leukemia: The mediating role of family functioning and resilience," *Cancers*, vol. 17, no. 3, p. 338, 2025, https://doi.org/10.3390/cancers17030338.

[2] M. S. Lajevardi *et al.*, "Dual roles of extracellular vesicles in acute lymphoblastic leukemia: implications for disease progression and theranostic strategies," *Medical Oncology*, vol. 42, no. 1, pp. 1-16, 2025, https://doi.org/10.1007/s12032-024-02547-7.

[3] N. Aziz *et al.*, "Analyzing Two Decades of Leukemia Mortality in the US (1999-2020)," *Clinical Lymphoma Myeloma and Leukemia*, 2025, https://doi.org/10.1016/j.clml.2025.03.006.

[4] R. Woudberg and E. Sinanovic, "Priority setting for improved leukemia management and research in South Africa: a modified Delphi study," *Cancer Causes & Control*, 2025, https://doi.org/10.1007/s10552-025-01979-4.

[5] G. Iacobellis, A. Leggio, C. Salzillo, S. Lucà, R. Ortega-Ruiz, and A. Marzullo, "Analysis and Historical Evolution of Paediatric Bone Tumours: The Importance of Early Diagnosis in the Detection of Childhood Skeletal Malignancies," *Cancers*, vol. 17, no. 3, p. 451, 2025, https://doi.org/10.3390/cancers17030451.

[6] V. Tanwar, B. Sharma, D. P. Yadav, and A. D. Dwivedi, "Enhancing Blood Cell Diagnosis Using Hybrid Residual and Dual Block Transformer Network," *Bioengineering*, vol. 12, no. 2, p. 98, 2025, https://doi.org/10.3390/bioengineering12020098.

[7] F. H. Najjar, S. Abd Kadum, and N. B. Hassan, "Integrating Multi-scale Feature Extraction into EfficientNet for Acute Lymphoblastic Leukemia Classification," *Journal of Image and Graphics*, vol. 13, no. 1, pp. 83-89, 2025, https://doi.org/10.18178/joig.13.1.83-89.

[8] A. Kumar and L. Nelson, "Deep Learning-based Blood Cell Classification using EfficientNetB3 Architecture," *2025 6th International Conference on Mobile Computing and Sustainable Informatics (ICMCSI)*, pp. 954-960, 2025, https://doi.org/10.1109/ICMCSI64620.2025.10883188.

[9] A. K. Abdulsahib, "Artificial Intelligence Based Deep Bayesian Neural Network (DBNN) Toward Personalized Treatment of Leukemia with Stem Cells," *Journal of Robotics and Control (JRC)*, vol. 3, no. 6, pp. 809-816, 2022, https://doi.org/10.18196/jrc.v3i6.16200.

[10] A. Shah, S. S. Naqvi, K. Naveed, N. Salem, M. A. Khan, and K. S. Alimgeer, "Automated diagnosis of leukemia: a comprehensive review," *IEEE Access*, vol. 9, pp. 132097-132124, 2021, https://doi.org/10.1109/ACCESS.2021.3114059.

[11] C. Pescia, A. M. Sozanska, E. Thomas, and R. A. Cooper, "Artificial intelligence in haematopathology: current perspective and future directions," *Diagnostic Histopathology*, 2025, https://doi.org/10.1016/j.mpdhp.2025.03.002.

[12] M.-A. Găman, M. Dugăeşescu, and D. C. Popescu, "Applications of Artificial Intelligence in Acute Promyelocytic Leukemia: An Avenue of Opportunities? A Systematic Review," *Journal of Clinical Medicine*, vol. 14, no. 5, p. 1670, 2025, https://doi.org/10.3390/jcm14051670.

[13] A. D. Rasamoelina, I. Cík, P. Sincak, M. Mach, and L. Hruška, "A large-scale study of activation functions in modern deep neural network architectures for efficient convergence," *Inteligencia Artificial*, vol. 25, no. 70, pp. 95-109, 2022, https://doi.org/10.4114/intartif.vol25iss70pp95-109.

[14] R. F. Oybek Kizi, T. P. Theodore Armand, and H.-C. Kim, "A Review of Deep Learning Techniques for Leukemia Cancer Classification Based on Blood Smear Images," *Applied Biosciences*, vol. 4, no. 1, p. 9, 2025, https://doi.org/10.3390/applbiosci4010009.

[15] J.-N. Eckardt *et al*., "Synthetic bone marrow images augment real samples in developing acute myeloid leukemia microscopy classification models," *npj Digital Medicine*, vol. 8, no. 1, p. 173, 2025, https://doi.org/10.1038/s41746-025-01563-9.

[16] R. Raj and A. Kos, "An Extensive Study of Convolutional Neural Networks: Applications in Computer Vision for Improved Robotics Perceptions," *Sensors*, vol. 25, no. 4, p. 1033, 2025, https://doi.org/10.3390/s25041033.

[17] A. Mjahad, A. Polo-Aguado, L. Llorens-Serrano, and A. Rosado-Muñoz, "Optimizing Image Feature Extraction with Convolutional Neural Networks for Chicken Meat Detection Applications," *Applied Sciences*, vol. 15, no. 2, p. 733, 2025, doi: https://doi.org/10.3390/app15020733.

[18] Y. Kim, K.-W. Lee, S. Lee, E. J. Woo, and K.-S. Hu, "Age-related morphological changes of the pubic symphyseal surface: using three-dimensional statistical shape modeling," *Scientific Reports*, vol. 15, no. 1, p. 494, 2025, https://doi.org/10.1038/s41598-024-84168-8.

[19] Y. Li *et al*., "Wheat growth stage identification method based on multimodal data," *European Journal of Agronomy*, vol. 162, p. 127423, 2025, https://doi.org/10.1016/j.eja.2024.127423.

[20] M. Ali *et al*., "Applications of Artificial Intelligence, Deep Learning, and Machine Learning to Support the Analysis of Microscopic Images of Cells and Tissues," *Journal of Imaging*, vol. 11, no. 2, p. 59, 2025, https://doi.org/10.3390/jimaging11020059.

[21] F. H. Najjar, K. T. Khudhair, Z. N. Khudhair, H. H. Alwan, and A. Al-khaykan, "Acute lymphoblastic leukemia image segmentation based on modified HSV model," *Journal of Physics: Conference Series*, vol. 2432, no. 1, p. 012020, 2023, https://doi.org/10.1088/1742-6596/2432/1/012020.

[22] A. Bilal, A. Alkhathlan, F. A. Kateb, A. Tahir, M. Shafiq, and H. Long, "A quantum-optimized approach for breast cancer detection using SqueezeNet-SVM," *Scientific Reports*, vol. 15, no. 1, p. 3254, 2025, https://doi.org/10.1038/s41598-025-86671-y.

[23] M. Almijalli, F. A. Almusayib, G. F. Albugami, Z. Aloqalaa, O. Altwijri, and A. S. Saad, "Automatic Active Contour Algorithm for Detecting Early Brain Tumors in Comparison with AI Detection," *Processes*, vol. 13, no. 3, p. 867, 2025, https://doi.org/10.3390/pr13030867.

[24] P. Kaur and P. Mahajan, "Detection of brain tumors using a transfer learning-based optimized ResNet152 model in MR images," *Computers in Biology and Medicine*, vol. 188, p. 109790, 2025, https://doi.org/10.1016/j.compbiomed.2025.109790.

[25] A. Rehman, N. Abbas, T. Saba, S. I. u. Rahman, Z. Mehmood, and H. Kolivand, "Classification of acute lymphoblastic leukemia using deep learning," *Microscopy Research and Technique*, vol. 81, no. 11, pp. 1310-1317, 2018, https://doi.org/10.1002/jemt.23139.

[26] A. E. Aby, S. Salaji, K. Anilkumar, and T. Rajan, "A review on leukemia detection and classification using Artificial Intelligence-based techniques," *Computers and Electrical Engineering*, vol. 118, p. 109446, 2024, https://doi.org/10.1016/j.compeleceng.2024.109446.

[27] P. K. Das, V. Diya, S. Meher, R. Panda, and A. Abraham, "A systematic review on recent advancements in deep and machine learning based detection and classification of acute lymphoblastic leukemia," *IEEE Access*, vol. 10, pp. 81741-81763, 2022, https://doi.org/10.1109/ACCESS.2022.3196037.

[28] S. I. U. Rahman *et al*., "Deep Learning and Artificial Intelligence-Driven Advanced Methods for Acute Lymphoblastic Leukemia Identification and Classification: A Systematic Review," *Computer Modeling*

in Engineering & Sciences (CMES), vol. 142, no. 2, pp. 1199-1231, 2025, https://doi.org/10.32604/cmes.2025.057462.

[29] F. Stagno *et al*., "Utilization of Machine Learning in the Prediction, Diagnosis, Prognosis, and Management of Chronic Myeloid Leukemia," *International Journal of Molecular Sciences*, vol. 26, no. 6, p. 2535, 2025, https://doi.org/10.3390/ijms26062535.

[30] Y. Xu *et al*., "Artificial intelligence: A powerful paradigm for scientific research," *The Innovation*, vol. 2, no. 4, p. 100179, 2021, https://doi.org/10.1016/j.xinn.2021.100179.

[31] A. Upadhyay *et al*., "Deep learning and computer vision in plant disease detection: a comprehensive review of techniques, models, and trends in precision agriculture," *Artificial Intelligence Review*, vol. 58, no. 3, pp. 1-64, 2025, https://doi.org/10.1007/s10462-024-11100-x.

[32] H. Naseri and A. A. Safaei, "Diagnosis and prognosis of melanoma from dermoscopy images using machine learning and deep learning: a systematic literature review," *BMC Cancer*, vol. 25, no. 1, p. 75, 2025, https://doi.org/10.1186/s12885-024-13423-y.

[33] H. Almahdawi, A. Akbas, and J. Rahebi, "Deep Learning Neural Network Based on PSO for Leukemia Cell Disease Diagnosis from Microscope Images," *Journal of Imaging Informatics in Medicine*, pp. 1-10, 2025, https://doi.org/10.1007/s10278-025-01474-x.

[34] F. R. T. Ferreira and L. M. do Couto, "Using deep learning on microscopic images for white blood cell detection and segmentation to assist in leukemia diagnosis," *The Journal of Supercomputing*, vol. 81, no. 2, pp. 1-42, 2025, https://doi.org/10.1007/s11227-024-06903-2.

[35] A. E. Aby, S. Salaji, K. Anilkumar, and T. Rajan, "Classification of acute myeloid leukemia by pre-trained deep neural networks: A comparison with different activation functions," *Medical Engineering & Physics*, vol. 135, p. 104277, 2025, https://doi.org/10.1016/j.medengphy.2024.104277.

[36] N. Gokulkrishnan, T. Nayak and N. Sampathila, "Deep Learning-Based Analysis of Blood Smear Images for Detection of Acute Lymphoblastic Leukemia," *2023 IEEE International Conference on Electronics, Computing and Communication Technologies (CONECCT)*, pp. 1-5, 2023, https://doi.org/10.1109/CONECCT57959.2023.10234824.

[37] K. A. Kadhim, F. H. Najjar, A. A. Waad, I. H. Al-Kharsan, Z. N. Khudhair, and A. A. Salim, "Leukemia classification using a convolutional neural network of AML images," *Malaysian Journal of Fundamental and Applied Sciences*, vol. 19, no. 3, pp. 306-312, 2023, https://doi.org/10.11113/mjfas.v19n3.2901.

[38] M. Hagar, F. K. Elsheref, and S. R. Kamal, "A new model for blood cancer classification based on deep learning techniques," *International Journal of Advanced Computer Science and Applications*, vol. 14, no. 6, 2023, https://doi.org/10.14569/IJACSA.2023.0140645.

[39] M. A. Rejula, S. Amutha, and G. Shilpa, "Classification of acute lymphoblastic leukemia using improved ANFIS," *Multimedia Tools and Applications*, vol. 82, no. 23, pp. 35475-35491, 2023, https://doi.org/10.1007/s11042-023-15113-6.

[40] M. Awais, R. Ahmad, N. Kausar, A. I. Alzahrani, N. Alalwan, and A. Masood, "ALL classification using neural ensemble and memetic deep feature optimization," *Frontiers in Artificial Intelligence*, vol. 7, p. 1351942, 2024, https://doi.org/10.3389/frai.2024.1351942.

[41] M. Awais, M. N. Abdal, T. Akram, A. Alasiry, M. Marzougui, and A. Masood, "An efficient decision support system for leukemia identification utilizing nature-inspired deep feature optimization," *Frontiers in Oncology*, vol. 14, p. 1328200, 2024, https://doi.org/10.3389/fonc.2024.1328200.

[42] A. Batool and Y.-C. Byun, "Lightweight EfficientNetB3 model based on depthwise separable convolutions for enhancing classification of leukemia white blood cell images," *IEEE access*, vol. 11, pp. 37203-37215, 2023, https://doi.org/10.1109/ACCESS.2023.3266511.

[43] L. K, N. R. B, P. M. A, S. S and K. M, "CapsENet: Deep Learning based Acute Lymphoblastic Leukemia Detection Approach," *2024 8th International Conference on I-SMAC (IoT in Social, Mobile, Analytics and Cloud) (I-SMAC)*, pp. 1577-1584, 2024, https://doi.org/10.1109/I-SMAC61858.2024.10714671.

[44] S. A. Preanto, M. T. Ahad, Y. R. Emon, S. Mustofa, and M. Alamin, "A study on deep feature extraction to detect and classify Acute Lymphoblastic Leukemia (ALL)," *arXiv*, 2024, https://doi.org/10.48550/arXiv.2409.06687.

[45] M. T. H. Khan Tusar, M. T. Islam, A. H. Sakil, M. Khandaker, and M. M. Hossain, "An Intelligent telediagnosis of acute lymphoblastic leukemia using histopathological deep learning," *Journal of Computing Theories and Applications*, vol. 2, no. 1, pp. 1-12, 2024, https://doi.org/10.62411/jcta.10358.

[46] M. T. H. K. Tusar and R. K. Anik, "Automated detection of acute lymphoblastic leukemia subtypes from microscopic blood smear images using Deep Neural Networks," *arXiv*, 2022, https://doi.org/10.48550/arXiv.2208.08992.

[47] G. Atteia, R. Alnashwan, and M. Hassan, "Hybrid feature-learning-based PSO-PCA feature engineering approach for blood cancer classification," *Diagnostics*, vol. 13, no. 16, p. 2672, 2023, https://doi.org/10.3390/diagnostics13162672.

[48] M. Aria, M. Ghaderzadeh, D. Bashash, H. Abolghasemi, F. Asadi, and A. Hosseini, "Acute lymphoblastic leukemia (ALL) image dataset," *Kaggle*, 2021, https://doi.org/10.34740/KAGGLE/DSV/2175623.

[49] M. Ghaderzadeh, M. Aria, A. Hosseini, F. Asadi, D. Bashash, and H. Abolghasemi, "A fast and efficient CNN model for B-ALL diagnosis and its subtypes classification using peripheral blood smear images," *International Journal of Intelligent Systems*, vol. 37, no. 8, pp. 5113-5133, 2022, https://doi.org/10.1002/int.22753.

[50] J. M. Choi and H. Chae, "moBRCA-net: a breast cancer subtype classification framework based on multi-omics attention neural networks," *BMC Bioinformatics*, vol. 24, no. 1, p. 169, 2023, https://doi.org/10.1186/s12859-023-05273-5.